18th Australasian Fluid Mechanics Conference
Launceston, Australia
3-7 December 2012

Stability of a Spring-Mounted Cantilevered-Free Flexible Plate in a Uniform Flow

R. M. Howell[1], **A. D. Lucey**[1] **& J. S. Kapor**[1]

[1]Fluid Dynamics Research Group
Curtin University of Technology
GPO Box U1987, Perth, WA 6845, Australia
Email: richard.howell@curtin.edu.au

Abstract

A new system in fluid-structure interaction (FSI) is studied wherein a cantilevered thin flexible plate is aligned with a uniform flow with the upstream end of the plate attached to a spring-mass system. This allows the entire system to oscillate in a direction perpendicular to that of the flow as a result of the mounting's dynamic interaction with the flow-induced oscillations, or flutter, of the flexible plate. While a fundamental problem in FSI, the study of this variation on classical plate flutter is also motivated by its potential as an energy-harvesting system in which the reciprocating motion of the support system would be tapped for energy production. In this paper we formulate and deploy a hybrid of theoretical and computational models for the fluid-structure system and map out its linear stability characteristics. The computational model detailed is a novel fully-implicit solution that is very robust to spatial and temporal discretisation. Compared to a fixed cantilever, the introduction of the dynamic support system is shown to yield lower flutter-onset flow speeds and a reduction of the order of the mode that yields the critical flow speed; these effects would be desirable for energy harvesting applications.

Introduction

Recent practical motivation for the renewed study of cantilevered-free flexible plates in axial flow - a problem first studied in the modern era by [8] - is the potential to use flow-induced oscillations, or flutter, of the flexible plate to capture kinetic energy from the mean flow. In the same way that musical instruments use string resonances to extract the required acoustic noise, these systems use resonances between the fluid and the structure from which useful energy can be obtained. Vortex-shedding from an upstream cylinder can be used to drive the dynamic deformation of the flexible plate, for example see [1] that principally operates at frequencies determined by the Strouhal number of the cylinder flow. Perhaps more versatile are the recent ideas in, for example, [12, 11] wherein it is the fluid-structure interaction of the flexible plate, or in the case of the latter reference an articulated beam, that is the source of its motions; these exploit the naturally occurring flutter instability of the flexible plate above a critical flow speed. In most of these studies the mechanical energy of the flexible-plate is converted to electrical energy via a piezoelectric material adhered to the surface of the flexible plate. This is both less convenient and robust than energy-harvesting systems in which the pitching and heaving of a rigid aerofoil drive reciprocating motion that can readily be converted into rotary motion of a shaft; for example see [13]. Many studies have also been made of extracting energy from the vortex-induced vibration or *galloping* of a rigid cylinder mounted on springs in a flow caused by *lock in* with the frequency of the cylinder's own downstream wake; for example see [2]. The advantage of these latter methods is that the energy can be extracted from the whole of the oscillating body and is not localised to the positioning of piezoelectric patches or dampers along the beam. The long-term goal of the present work is the development of an energy-harvesting system that combines the merits of the flexible-plate flutter systems with the robust energy transmission principles of rigid-aerofoil systems. We therefore conceive the system illustrated in figure 1 wherein the flow-induced oscillations of the flexible plate drive vertical oscillatory motion of a mass-spring support system having its own dynamics that can clearly be tuned. The extraction of power could readily be modelled by the inclusion of linear damping at the support. However, the first step towards our goal is to understand the stability characteristics of this new fundamental FSI system. Importantly, we note that this system also has the capacity to elucidate further understanding of the snoring phenomenon, capturing the dynamics of the fluttering uvula mounted on the flexible yet constrained soft palate, see [4]. In this paper we therefore develop a theoretical and computational model of the two-dimensional system, leave damping to one side, and map out the dynamics of the remaining parameter space that we find has the usual non-dimensional control parameters, mass ratio $\bar{L}$ and flow speed $\bar{U}$, for a fixed cantilever, in addition to which there are the natural frequency of the spring-mass support system, $\bar{\omega}_s$, and the length of the rigid-inlet $\bar{L}_s$ which is maintained at zero-length in this study. To this end, the method of [6] that mixed numerical simulation with eigenvalue analysis is built upon in [5]; herein we present the key points of the latter study with some new theoretical developments. Thus, ideal two-dimensional flow is assumed wherein the rotationality of the boundary-layers is modelled by vortex elements on the solid-fluid interface and the imposition of the Kutta condition at the plate's trailing edge. The Euler-Bernoulli beam model is used for the structural dynamics. The latter is appropriate because it is our overall objective to design and optimise an energy-harvesting system that operates for low-amplitude deformations - to reduce material fatigue effects - of the flexible plate by tuning the support system such that the available wind speed coincides with the critical speed of flutter onset of the flexible plate. The results presented in this paper demonstrate that this strategy is practicable.

Theoretical & Computational Modelling

The essential modelling is described in detail in [6] wherein the system of figure 1 was mounted rigidly and symmetrically within a channel with its walls located at $y = \pm H$; the present system is obtained by letting $H \to \infty$. For the present paper, we also neglect the effects of the wake that were modelled in the precursor paper. Further essential model modifications

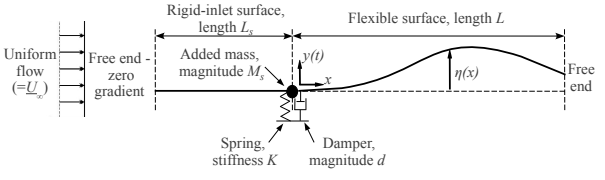

Figure 1: The fluid-structure system under consideration.

are detailed in [5] to incorporate the mobile-cantilever; a brief overview of the theory in these two papers is detailed below. Simply supported free beams where the support can move vertically and actuate the system have been analysed in studies of insect flight and base-excited, fluid-conveying flexible tubes, for example see [10] and [3] respectively, and constrain that the leading edge must follow (i) the heaving motion and (ii) the pitching motion of the actuating force. In our study as well as applying an actuating force due to the reaction of the spring, we allow that the motion of the leading edge can also be actuated by the motion of the flexible plate; we therefore modify these constraints so that they are applied through the inclusion of (i) a non-zero normal velocity at all panel control points equal to the velocity of the first mass point (upstream end of the flexible plate), and (ii) a shear-force balance condition at the leading edge that transmits the shear force that drives the vertical motion of the mounting system and the rigid, upstream splitter-plate whilst also enforcing that neither free nor controlled rotation of the beam about its leading edge is permitted; this means that the support mechanism can provide, without deformation, any level of moment reaction to the flexible plate at its upstream end.

We now summarise the approach of [5] as applied to the present investigation and show how these two conditions for the spring mass system are readily incorporated in the model. The flow field is found using a linearised boundary-element method (BEM) with quantity N first-order vortex panels on the flexible plate because of the discontinuity of tangential fluid velocity across the plate that makes it a lifting surface; the distributed lift drives the motion of the flexible plate. The singularity strengths are determined by enforcing the no-flux boundary condition at every panel control point and continuity of the distributed vorticity between adjacent panels in the discretisation. However, enforcing condition (i) from above requires that the no-flux condition be modified because all the panels now move with an additional component of normal velocity $\dot{\eta}_1$, η being the displacement of the plate. In addition the boundary condition of zero vorticity at the plate's trailing edge is applied, thus enforcing the standard Kutta condition of zero pressure difference at the trailing edge for linear displacements. We now introduce the two equations that govern the system: the first utilises the unsteady Bernoulli equation for panels $2-N$ to determine the pressure distribution on the flexible plate. The transmural pressure is then used as the forcing term in the one-dimensional thin flexible-plate equation couched in finite-difference form. The motions of the plate and the fluid flow are fully coupled through deflection, vertical velocity and acceleration of the two media at their interface. This allows the following single system (matrix) equation to be written

$$\begin{aligned} \rho h\,[\mathbf{I}]\,\{\ddot{\eta}+\ddot{\eta}_1\}+B\,[\mathbf{D_4}]\,\{\eta\} &= 2\rho_f U_\infty^2 \frac{1}{\delta x}\left[\mathbf{B_1^+}\right]\{\eta\} \\ + \quad \rho_f U_\infty \left[\mathbf{B_1^-}+\mathbf{B_{1^*}^-}\right]\{\dot{\eta}\} &+ \rho_f U_\infty \frac{1}{\delta x}\left[\mathbf{B_2^+}\right]\{\dot{\eta}\} \\ &+ \rho_f\left[\mathbf{B_2}+\mathbf{B_{2^*}}\right]\{\ddot{\eta}\}, \quad (1) \end{aligned}$$

where $[\mathbf{B}]$ are matrices of singularity influence coefficients, $[\mathbf{D_4}]$ is a fourth-order spatial-differentiation matrix and $[\mathbf{I}]$ is the identity matrix. The $[\mathbf{B}]$ matrices marked with a $+$ or $-$ have been suitably rearranged to have the equations in terms of η instead of panel angle θ; those marked with an asterisk $*$ are the additional effects of the mobile mounting and only contain values in their first column. ρ, h, and B are respectively, the material density, thickness and flexural rigidity of the plate, the dynamics of which appear on the left-hand side of the equation. The extra $\ddot{\eta}_1$ in the first mass term on the left-hand side reflects the extra inertia of the system owing to the moving neutral axis. Uniform discretisation of the plate length L into the N collocation points defines $\delta x = L/N$. The pressure perturbation that drives the plate motion appears on the right-hand side, where ρ_f is the fluid density. The pressure terms that depend on plate displacement, velocity and acceleration in equation (1) can be interpreted as the hydrodynamic stiffness, damping and inertia respectively. For $N = 1$ condition (ii) will be applied as the upstream-end condition where the shear force drives the vertical motion of the mounting system and the rigid-upstream splitter plate. Thus, the shear force in the flexible plate is calculated through the following equation of motion for $\eta_1(t)$,

$$M\frac{\partial^2\eta_1}{\partial t^2}+d\frac{\partial\eta_1}{\partial t}+K\eta_1 = \frac{Eh^3}{12}\frac{\partial^3\eta}{\partial x^3}|_{x=0}+\int_{-L_s}^{0}\delta p_s dx, \quad (2)$$

and where $\eta(x,t)$ is the flexible-plate vertical-displacement field; M is the actual mass of the first mass point $\rho h\delta x$, K is the spring stiffness, d a dashpot-type damping coefficient (zero in the present results) and δp_s is the pressure difference across the moving splitter plate that generates an additional vertical force driving the motion of the support system. The shear condition therefore joins two separate systems: a vertically oscillating flat plate with a vertically oscillating flexible plate. It is also noted that the first mass point in the system is constrained to be horizontal leading to a flat panel in the BEM and therefore an absence of hydrodynamic stiffness on this panel as well as along the rigid inlet; it is effectively an extension of the rigid inlet and therefore the pressure on this panel is included the value of δp_s on the right hand side of equation (2). We therefore have the following values for the boundary condition mass points

$$\eta_{-1}=\eta_0=\eta_1, \quad \dot{\eta}_0=\dot{\eta}_1 \quad \text{and} \quad \ddot{\eta}_0=\ddot{\eta}_1. \qquad (3a, b, c)$$

The conditions of equation (3) are applied in the leading-edge values of spatial derivative and influence coefficient properties in equations (1) and (2).

We take two approaches to the solution of the system comprised of equations (1) and (2) rearranged as the system

$$\{\ddot{\eta}\}=[\mathbf{E}]\{\dot{\eta}\}+[\mathbf{F}]\{\eta\}, \quad (4)$$

where $[\mathbf{E}]$ and $[\mathbf{F}]$ are readily inferred from equations (1) and (2). In the first we reduce the second-order ordinary differential equation in $\{\eta\}$ to first-order using the state-space variables $w_1(t)=\eta(t)$ and $w_2(t)=\dot{\eta}(t)$. Rearranging in companion-matrix form, single-frequency time-dependent response is assumed at ω which is a complex eigenvalue of the companion-form $[H]$. Positive ω_I and ω_R respectively represent the oscillatory and amplifying parts of the response. As the flexible plate is discretised into N mass points we therefore extract $2N$ system eigenmodes. Alternatively, we perform a time-discretisation of the system and then numerically time-step the equation using a novel fully-implicit method to determine the system response to an applied form of initial perturbation. This method was detailed in [7] for potential flow over a one-sided hinged-hinged beam. In doing so we are able to study transient behaviour and reveal localised flow-structure dynamics that when summed contribute to the system response. The method is summarised as follows: to calculate next time step values for beam velocity and displacement we use standard second-order trapezoidal approximations

$$\dot{\eta}^{t+1} = \dot{\eta}^t+\frac{\delta t}{2}\ddot{\eta}^{t+1}+\frac{\delta t}{2}\ddot{\eta}^t, \quad (5)$$

$$\eta^{t+1} = \eta^t+\frac{\delta t}{2}\dot{\eta}^{t+1}+\frac{\delta t}{2}\dot{\eta}^t. \quad (6)$$

It is noted that beam properties without the subscript t are values from the previous time step. Entering equations (5) and (6) into equation (4) we have the following formulation for the beam acceleration

$$\left\{\ddot{\eta}^{t+1}\right\}=\left[[\mathbf{I}]-\frac{\delta t^2}{4}[\mathbf{F}]-\frac{\delta t}{2}[\mathbf{E}]\right]^{-1}\left\{\left[\delta t\,[\mathbf{F}]+[\mathbf{E}]\right]\{\dot{\eta}^t\}+\right.$$

$$[\mathbf{F}]\{\eta^t\} + \left[\frac{\delta t^2}{4}[\mathbf{F}] + \frac{\delta t}{2}[\mathbf{E}]\right]\{\ddot{\eta}^t\}\Big\}. \qquad (7)$$

The result of equation (7) is calculated at the beginning of each time step; the result is then used to calculate beam velocity in equation (5) and finally this result is then used to solve for beam displacement using equation (6). The method is very robust to spatial and temporal discretisation and requires only a single or double iteration per time step to converge. It is noted that this method is only applicable to linear deflections of a linearised or non-linear system.

Results

Our results are presented in non-dimensional form having used the scheme in [9] whereby reference time and length are

$$t_r = (\rho h)^{\frac{5}{2}}/(\rho_f^2 B^{\frac{1}{2}}) \text{ and } L_r = \rho h/\rho_f, \qquad (8a, b)$$

and therefore

$$\bar{t} = t/t_r \text{ and } \bar{U} = U_\infty t_r/L_r. \qquad (9a, b)$$

The non-dimensional streamwise coordinate, the length (or mass ratio) of the flexible plate and the non-dimensional rigid inlet length are defined by

$$\bar{x} = x/L, \quad \bar{L} = L/L_r \text{ and } \bar{L}_s = L_s/L. \qquad (10a, b, c)$$

This scheme permits $\bar{U}$ and $\bar{L}$ to be interpreted respectively as the physical flow speed and plate length for given fluid and plate properties. Instead of using the non-dimensional form of the mounting's stiffness coefficient $\bar{K}$ associated with the foregoing scheme, we use the following property from systems analysis

$$\bar{\omega}_s = (K/M_T)^{\frac{1}{2}} t_r, \qquad (11)$$

where $\bar{\omega}_s$ is the non-dimensional natural frequency of the spring-mass system. M_T is equal to ρhL, the entire mass of the plate being critical to the spring-mass system's natural frequency; the effect of the fluid mass along the flexible and rigid surfaces on the natural frequency is accounted for in the non-dimensional scheme. In summary, we find that the critical velocity of the system $\bar{U}_c$ takes the functional dependence on the system's control parameters

$$\bar{U}_c = f(\bar{L}, \bar{L}_s, \bar{\omega}_s). \qquad (12)$$

Figure 2 shows the results for a homogeneous, or 'standard', short plate at $\bar{L} = 1$ with $\bar{L}_s = 0$ and $\bar{\omega}_s = 1$. Figure 2a shows the variation of system eigenvalues with applied flow speed. The broken lines denote the oscillatory (imaginary) part of the eigenvalue, ω_I, while the solid lines show the associated growth/decay (real) part of the eigenvalue, ω_R. The modes are numbered in the plots following their order of increasing frequency at zero flow speed. Instability sets in at the lowest flow speed (the critical flow speed, $\bar{U}_c$) for which ω_R becomes positive, *i.e.* that at which the ω_R locus crosses the horizontal axis to move into the upper positive quadrant of the plot. In figure 2a it is seen that single-mode flutter of the second system mode - highlighted by a thicker line type - is the critical instability at a non-dimensional flow speed $\bar{U} = \bar{U}_c = 5.6$. Figure 2b shows a numerical simulation of the critical mode at this flow speed. The simulation was started by releasing the plate from an applied deformation - the thick black line - in the shape of the first *in-vacuo* mode. The critical mode, seen to contain strong contributions from the first and second *in-vacuo* modes, then evolves from the initial excitation. Contrasting figure 2b with the equivalent fixed-cantilever result in [6] for $\bar{H} = 1$ (for

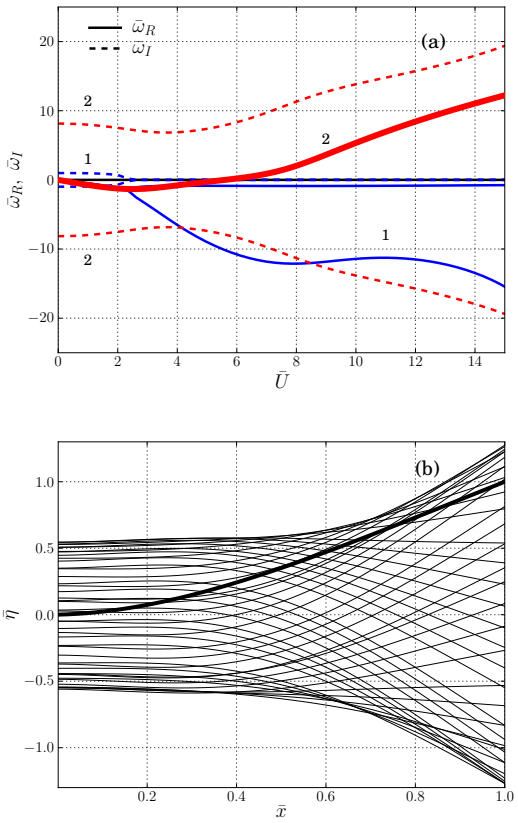

Figure 2: System dynamics for $\bar{L} = 1$ and $\bar{L}_s = 0$ with $\bar{\omega}_s = 1$: (a) Variation of numbered eigenvalues with flow speed (oscillatory and growth/decay parts represented by broken and full lines respectively) with the real part of Mode 2 that becomes unstable highlighted through a thicker line type, (b) time-sequence of instantaneous plate position at $\bar{U}_c = 5.6$ (the thick line being the initial deflection with early oscillations removed).

which the channel walls were shown to exert negligible effect) shows that for the fixed cantilever the critical mode shape loses most of its first-order mode content and becomes more second-mode dominated. The reason for this is the loss of the stronger real component of the first mode just below the x-axis seen in figure 2a. For this reason the simulation in [6] was started by releasing the plate from an applied deformation in the shape of the second *in-vacuo* mode enabling the system to settle more quickly into its neutrally-stable oscillation. It is noted that the mobile cantilever instability is more severe than the equivalent instability in [6] as the former has a steeper gradient of the real part of Mode 2 when it becomes positive. Figure 3a shows how the critical speeds of instability onset vary with the spring-mounting characterised by $\bar{\omega}_s$ for fixed $\bar{L}$ with $\bar{L}_s = 0$ while figure 3b shows the corresponding variation of the frequencies of the critical modes. The vertical dashed lines show the $\bar{U}_c$ and $\bar{\omega}$ values for the fixed cantilever case. In figure 3 the system is always destabilised by single-mode flutter. We remark that the detailed result of figure 2 appears as the data point for $\bar{\omega}_s^{-1} = 1$ in figure 3. Figure 3a shows that the spring-mounted cantilever is typically less stable - critical flow speeds are lower - than for the fixed cantilever. Figure 3b shows that the introduction of the spring-mounting decreases the oscillation frequencies of the critical mode as compared with the fixed-cantilever. The onset flow speeds and frequencies of the critical mode are seen to approach those of the fixed cantilever as $\bar{\omega}_s$ is increased ($\bar{\omega}_s^{-1}$ is

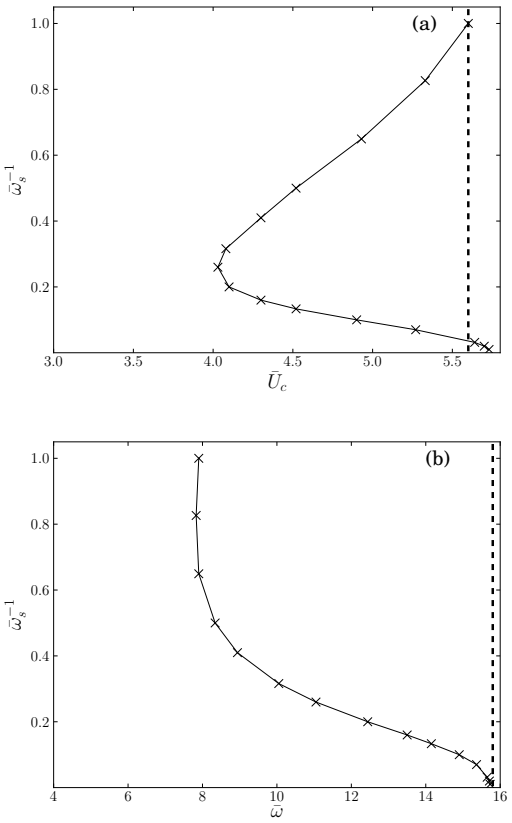

Figure 3: Zero-gradient-free beam at $\bar{L} = 1$ and $\bar{L}_s = 0$: Plots of $\bar{\omega}_s^{-1}$ against (a) $\bar{U}_c$ and (b) $\bar{\omega}$. Single-mode flutter; dashed lines denote $\bar{U}_c$ and $\bar{\omega}$ at $\bar{U}_c$ for the fixed cantilever case.

decreased) although a very small numerical difference between the new mobile and previous [6] fixed cantilever models appears in figure 3a. This is most probably due to ill-conditioning of the system stiffness matrix as the value of the spring-support coefficient is made extremely large. The most significant feature of figure 3a is that there exists a minimum value of critical speed. This is due to switching of the critical mode. Thus, as $\bar{\omega}_s$ is decreased in figure 3a the lower branch is principally characterised by Mode-2 content typified in [6] whereas the upper branch is dominated by Mode-1 content as typified by figure 2b. This effect - the reduction of critical-mode order - is reflected in the reduction of critical mode frequency seen in figure 3b as $\bar{\omega}_s$ is reduced.

Conclusions

We have developed a model for predicting the two-dimensional linear-stability characteristics of a spring-mounted cantilevered flexible plate in a uniform flow. The basic stability characteristics of the system have been investigated for cases without a rigid upstream splitter plate that, for a rigid mounting, would succumb to single-mode flutter. It has been shown that the introduction of a spring-mounting is generally destabilising in that it leads to lower values of the critical flow speed of the onset of both types of flutter. As the natural frequency of the mounting system is reduced, a value is reached for which the critical speed is a minimum. This minimum exists because the critical mode evolves from one of a higher to a lower order that can then become more stable with further decreases to the mounting stiffness. In effect the flexible plate becomes very stiff as compared with the mounting system and the entire system then asymptotes towards rigid-body motion of the plate and support. These stability findings augur well for the introduction of means to extract power from the reciprocating motion of the support; this is readily modelled by introducing a dashpot damper alongside the spring. The present methods could then be used to determine optimal system parameters for energy harvesting.

References

[1] Allen, J. J. and Smits, A. J., Energy harvesting eel, *Journal of Fluids and Structures*, **15**, 2001, 629–640.

[2] Barrero-Gil, A., Alonso, G. and Sanz-Andres, A., Energy harvesting from transverse galloping, *Journal of Sound and Vibration*, **329**, 2010, 2873–2883.

[3] Chang, G. H. and Modarres-Sadeghi, Y., Flow-induced oscillations of a cantilevered pipe conveying fluid with a base excitation, in *Proceedings 10th International Conference on Flow-Induced Vibration (& Flow-Induced Noise)*, Dublin, Ireland, 2012, 15–19.

[4] Elliott, N. S. J., Lucey, A. D., Heil, M., Eastwood, P. R. and Hillman, D. R., Modelling and simulation of fluid-structure interactions in human snoring, in *Proceedings 19th International Congress on Modelling and Simulation*, Perth, Australia, 2011.

[5] Howell, R. M. and Lucey, A. D., The fluid-structure interaction of a spring-mounted cantilevered-free flexible plate in a uniform flow, in *Proceedings 10th International Conference on Flow-Induced Vibration (& Flow-Induced Noise)*, Dublin, Ireland, 2012, 219–226.

[6] Howell, R. M., Lucey, A. D., Carpenter, P. W. and Pitman, M. W., Interaction between a cantilevered-free flexible plate and ideal flow, *Journal of Fluids and Structures*, **25**, 2009, 544–566.

[7] Kapor, J. S., Lucey, A. D. and Pitman, M. W., A mesh-free compliant-wall fluid-structure interaction model, in *Proceedings 19th International Congress on Modelling and Simulation*, Perth, Australia, 2011.

[8] Kornecki, A., Dowell, E. H. and O'Brien, J., On the aeroelastic instability of two-dimensional panels in uniform incompressible flow, *Journal of Sound and Vibration*, **47**, 1976, 163–178.

[9] Lucey, A. D., Sen, P. K. and Carpenter, P. W., Excitation and evolution of waves on an inhomogeneous flexible wall in a mean flow, *Journal of Fluids and Structures*, **18**, 2003, 251–267.

[10] Manela, A., Vibration and sound of an elastic wing actuated at its leading edge, *Journal of Sound and Vibration*, **331**, 2012, 638–650.

[11] Singh, K., Michelin, S. and de Langre, E., Energy harvesting from axial fluid-elastic instabilities of a cylinder, *Journal of Fluids and Structures*, **30**, 2012, 159–172.

[12] Tang, L., Païdoussis, M. P. and Jiang, J., Cantilevered flexible plates in axial flow: Energy transfer and the concept of flutter mill, *Journal of Sound and Vibration*, **326**, 2009, 263–276.

[13] Zhu, Q. and Peng, Z., Mode coupling and flow energy harvesting by a flapping foil, *Physics of Fluids*, **21**, 2009, 033601–(1–10).